GEOCHEMISTRY

Photoreduction of inorganic carbon(+IV) by elemental sulfur: Implications for prebiotic synthesis in terrestrial hot springs

Yanzhang Li[1,2]*, Yan Li[1,2]*†, Yi Liu[1,2], Yifu Wu[1,2], Junqi Wu[1,2], Bin Wang[3], Huan Ye[1,2], Haoning Jia[1,2], Xiao Wang[1,2], Linghui Li[1,2], Meixiang Zhu[1,2], Hongrui Ding[1,2], Yong Lai[1,2], Changqiu Wang[1,2], Jeffrey Dick[4], Anhuai Lu[1,2,4]†

Terrestrial hydrothermal systems have been proposed as alternative birthplaces for early life but lacked reasonable scenarios for the supply of biomolecules. Here, we show that elemental sulfur (S^0), as the dominant mineral in terrestrial hot springs, can reduce carbon dioxide (CO_2) into formic acid (HCOOH) under ultraviolet (UV) light below 280 nm. The semiconducting S^0 is indicated to have a direct bandgap of 4.4 eV. The UV-excited S^0 produces photoelectrons with a highly negative potential of −2.34 V (versus NHE, pH 7), which could reduce CO_2 after accepting electrons from electron donors such as reducing sulfur species. Simultaneously, UV light breaks sulfur bonds, benefiting the adsorption of charged carbonates onto S^0 and assisting their photoreduction. Assuming that terrestrial hot springs covered 1% of primitive Earth's surface, S^0 at 10 μM could have produced maximal 10^9 kg/year HCOOH within 10-cm-thick photic zones, underlying its remarkable contributions to the accumulation of prebiotic biomolecules.

INTRODUCTION

The origin of life remains unsolved but can be summarized as organic monomers formed, accumulated, assembled, developed into complex polymers and, finally, living beings (*1*–*4*). A critical step is the prebiotic synthesis of simple organic molecules represented by formic acid, acetic acid, pyruvate, and amino acids from inorganic carbon sources. This process must have sustainably supplied base materials for further inoculation of complex life substances, which ultimately developed into primitive life forms (*2*, *5*, *6*). The pathways and environments that could have given rise to primitive organic molecules, therefore, are of great importance and have been the subject of many models and hypotheses.

One hypothesis of interest is that the terrestrial origin of life and nascent life emerged in vapor-dominated zones of inland geothermal systems (*7*–*10*). Unlike submarine hydrothermal vents, the geothermal fluids that well up from terrestrial hot springs develop on land or in shallow pools, accompanied with volcanic landmasses, geysers, and steam vents. With the discovery of hyperthermophiles as well as thermal, pH, and chemical redox gradients (*10*–*12*), terrestrial hydrothermal systems are also regarded as a likely environment for abiogenesis and even the cradle of early life. However, the initial biological records in terrestrial systems are not well preserved because of long-term geological and anthropogenic activities. The earliest signs of life on land (~3.5 billion years ago) discovered in Western Australia (*13*) could be regarded as an evidence for early life's possible origin in terrestrial hydrothermal environment. Nevertheless, until now, there has been no convincing experimental model for the creation of necessary organic molecules from terrestrial inorganics.

Notably, early aqueous environments including the pools and springs developing in terrestrial hydrothermal systems are presumed to involve considerable carbonates [H_2CO_3, HCO_3^-, and CO_3^{2-}, denoted as carbon(+IV)], which were formed by the dissolution of atmospheric CO_2 that was present at high concentration (*14*, *15*). Whether organics could be synthesized from these inorganic carbon species is an important issue and worth further exploration, wherein minerals have been suggested to play key roles (*3*, *6*, *16*–*19*). In particular, semiconducting sulfide minerals present in hydrothermal systems, like sphalerite (ZnS) and alabandite (MnS), were demonstrated to be able to catalyze the reduction of CO_2 and the synthesis of primitive biomolecules under ultraviolet (UV) light (*20*, *21*). These semiconducting metal sulfides have thus been suggested as the key to unravel the puzzle of life's origin in terrestrial hot springs (*7*). However, in the primitive Earth, a majority of sulfide minerals were deposited at deep-sea subduction zones and ridges (*22*). A few of them with low solubility precipitated at terrestrial hydrothermal systems, while those that precipitated slowly like ZnS and MnS were suggested to be enriched in far-off ponds and puddles away from hot springs, fed by downstream and cooled fluids (*7*). Therefore, it is very probable that the origin of life in early terrestrial hydrothermal systems is dominated by another unrevealed mineral model.

In modern volcanic hydrothermal systems on the surface of Earth, elemental sulfur (S^0) is a quite abundant mineral (*23*–*26*). It was also the main product of photochemical or comproportionation reactions that involved −2 and +4 valent sulfur in the primitive Earth (*27*–*29*). The discharged hydrogen sulfide (H_2S) and sulfur dioxide (SO_2) gas from prebiotic craters and hydrothermal vents were substantial and estimated to be over three times as abundant as those from modern volcanos (*28*, *30*, *31*). The production rate of S^0 aerosol in a proposed model reached about 10^7 molecules cm^{-2} s^{-1}; some of these aerosols could have condensed into

[1]Beijing Key Laboratory of Mineral Environmental Function, School of Earth and Space Sciences, Peking University, Beijing 100871, People's Republic of China. [2]The Key Laboratory of Orogenic Belts and Crustal Evolution, School of Earth and Space Sciences, Peking University, Beijing 100871, People's Republic of China. [3]Sinopec Beijing Research Institute of Chemical Industry, Beijing 100013, People's Republic of China. [4]The Key Laboratory of Metallogenic Prediction of Nonferrous Metals and Geological Environment Monitoring, School of Geosciences and Info-Physics, Central South University, Changsha 410083, People's Republic of China.
*These authors contributed equally to this work.
†Corresponding author. Email: liyan-pku@pku.edu.cn (Y.L.); ahlu@pku.edu.cn (A.L.)

particles and then dropped into the early ocean (*30*). Therefore, a scenario in which natural S^0 was immersed in the carbonate environment, especially in terrestrial hydrothermal systems, was likely to exist in the prebiotic Earth. However, S^0 has rarely been an attractive catalyst or reactant but was rather deemed a negligible by-product in atmospheric or aquatic photochemistry (*27*, *30*). As a typical nonmetallic semiconducting mineral (*32*), whether S^0 could photocatalyze some prebiotic synthesis reactions and thus contribute to the chemical origin of life has not yet been reported and elucidated.

In this study, we provide experimental evidence for the photocatalytic production of HCOOH in a simplified terrestrial hydrothermal system with dissolved carbonate and suspended S^0. The semiconducting and photoelectrochemical properties of S^0 are systematically investigated, and the results support the model that sufficient photoelectrons with highly reducing potentials are excited to enable CO_2 reduction under UV light. In addition, UV light is shown to break the sulfur bonds of S^0, which favors the adsorption of carbonate anions onto S^0 and thus facilitates charge transfer. This study highlights the remarkable role of semiconducting S^0 in converting carbon(+IV) into organics and supports a possible pathway for biomolecule accumulation in terrestrial hydrothermal systems. The distinguished highly reducing photoelectrons from UV-excited S^0 could be further extended to synthesize more complicated organics, thus playing comparable roles to the traditional highly reducing agent like H_2 and high temperature–dependent pathway in hydrothermal systems.

RESULTS

Geochemistry of Tengchong terrestrial hot spring with abundant S^0

Tengchong geothermal field, located in Yunnan Province in southwestern China, is famous for its Cenozoic volcanism and present-day geothermal features. In these active hot springs and pools (58° to 97°C) exposed on the surface of Earth, massive S^0 with characteristic yellow color was observed to deposit along the margin of the hot pool below the water's surface (Fig. 1, A and B). Mineral phase identification by x-ray diffraction revealed orthorhombic α-sulfur (homocyclic S_8, which is the most stable form of S^0) as the main component in the submerged yellow deposit, accompanied with griceite (LiF) and amorphous geyserite (Fig. 1C). Some white deposits, however, lacking S^0 and consisting of thenardite (Na_2SO_4), halite (NaCl), griceite, and geyserite, were deposited beyond the spring water (Fig. 1,B and C). At some fumaroles without charging water, a small amount of S^0 was deposited on the surface of porous siliceous sinter (Fig. 1D). Under scanning electron microscopy (SEM), the S^0 mineral in hot springs had a crystal size of several micrometers that did not show fixed crystal shape (Fig. 1, E and F). In comparison, the S^0 at fumaroles was present in bigger and well-crystallized druses (Fig. 1D). Multiple ions, mainly including Na^+, K^+, Mg^{2+}, Li^+, Cl^-, S^{2-}, and SO_4^{2-}, were detected in all six sampling sites (table S1). The ascending H_2S gas could maintain a reducing environment for the preservation of S^0 in the water. The white deposits, which were dominated by sulfates and were not immersed in reducing water, therefore, were the oxidation products of the yellow deposits. As can be seen from above observations, one of

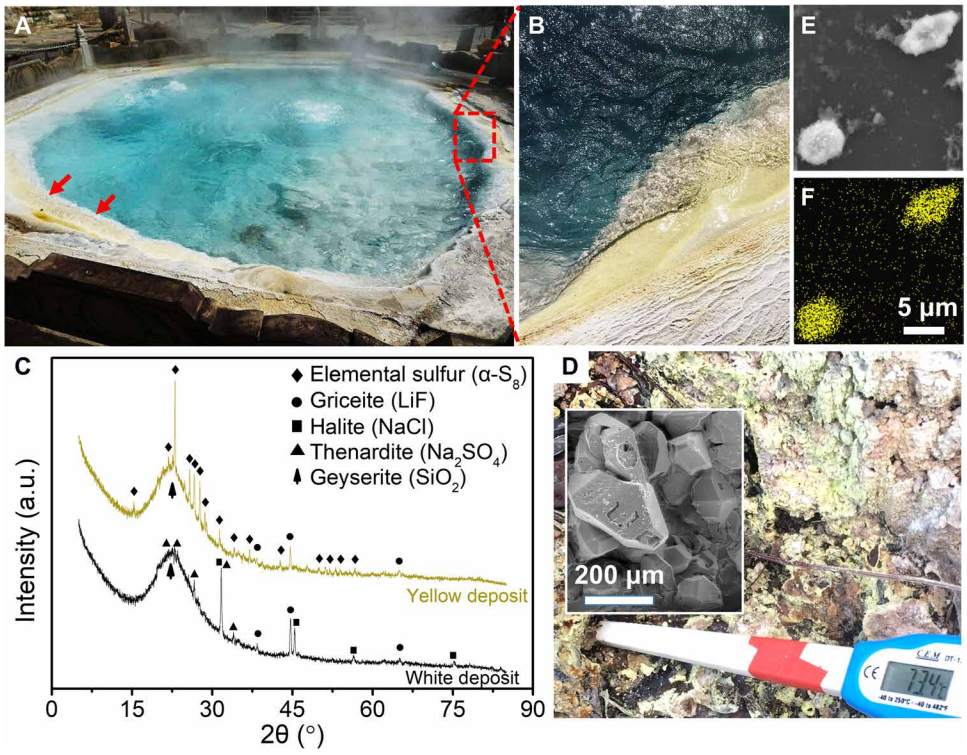

Fig. 1. The occurrence of S^0 at a geothermal field in Tengchong, China. (**A**) A degassing spring named Dagunguo (96°C, pH 8.0) that is 5 m in diameter with S^0 deposition labeled by red arrows. (**B**) S^0 at the poolside and in the hot water. (**C**) X-ray diffraction patterns of yellow and white deposits collected from (B). a.u., arbitrary unit. (**D**) Active fumarole with abundant S^0, siliceous sinter, and salt deposition (the digital thermometer shows 73.4°C). Inset: Well-crystallized S^0 druse observed by SEM. (**E**) SEM image of S^0 particles collected in hot springs. (**F**) Sulfur element mapping pattern at S Kα line corresponding to the region in (E). Photo credit: Y.W., Peking University.

the most remarkable features in the terrestrial hydrothermal system is the deposition and suspension of S^0 in the sunlit and spring water.

Photoreduction of carbonate to produce HCOOH in the presence of S^0

The photochemical reactions were conducted in three control systems: system 1 with S^0 and UV light, system 2 with S^0 and visible light, and system 3 with UV light only. As the reaction progressed, HCOOH was continuously produced only in system 1 (Fig. 2A and fig. S1), while no HCOOH was detected in either system 2 or system 3. The amounts of HCOOH increased along with the concentration of carbon(+IV) and S^0 (Fig. 2B). After irradiation for 12 hours, 2.6 mM HCOOH was produced in the solution containing 50 mM $NaHCO_3$ and S^0 (5 g/liter).

In the presence of both S^0 and UV light, the total yields of HCOOH after 12 hours were 0.6, 2.6, 0.8, and 0.2 mM at pH 4, 6, 8, and 10, respectively (Fig. 2C). Notably, the chemical forms of carbonate species drastically varied with pH. The H_2CO_3 or HCO_3^- dominated systems (99 and 97% in pH 4 and 8, respectively) produced moderate HCOOH, while the system with 61% CO_3^{2-} and 39% HCO_3^- (pH 10) produced the minimum. The highest yields of HCOOH, unexpectedly, occurred in a weakly acidic system (pH 6) with 64% H_2CO_3 and 36% HCO_3^-, suggesting that both H^+ and HCO_3^- were crucial to carbon(+IV) reduction in this case.

Controlled experiments were conducted under three monochromatic wavelengths: 254, 313, and 365 nm, corresponding to UVC (200 to 280 nm), UVB (280 to 320 nm), and UVA (320 to 400 nm), respectively. Notably, HCOOH was only produced under 254-nm irradiation, and its yields were positively correlated with light intensity (Fig. 2D). The incident photon-to-current conversion efficiency (IPCE) under 254-nm irradiation was calculated to be 7.6, 7.0, 6.1, and 4.5‰, corresponding to a light intensity of 0.25, 0.50, 0.75, and 1.00 mW/cm^2, respectively (Fig. 2D). All the above results suggested that the production of HCOOH required the involvement of both S^0 and UVC light, and its yielding rate was correlated with the concentrations of C(+IV) and S^0 (Fig. 2B), pH (Fig. 2C), and light intensity (Fig. 2D).

The photoactivity of S^0 under UV light

Production of photoelectrons

The optical absorption spectra of S^0 showed different patterns at 25° and −200°C (Fig. 3A). At room temperature, a clear absorption edge emerged in the visible band (Fig. 3A) and its onset was 475 nm (λ_1). When the sample was cooled down to −200°C, the absorption edge moved to 280 nm (λ_2), while the previous edge at 475 nm disappeared (Fig. 3A). It was reported that the color of S^0 changes from yellow to white at low temperature (*33*). The absorption spectra confirmed this behavior and suggested that the optical absorbance of S^0 is temperature dependent. In terms of its emission spectra, dual fluorescence signals were observed to be situated almost at the center of two absorption edges (Fig. 3A). Therefore, S^0 should have two types of electronic transition, denoted as transition I and transition II, which occur under visible and UV light, respectively. The band structure calculation based on density functional theory (DFT) proves that S^0 (in the form of orthorhombic S_8) is an indirect semiconductor with a narrow indirect bandgap and a wide direct bandgap (fig. S2). Transition I in Fig. 3A is assigned to the indirect mode, which absorbs parts of visible light (λ < 475 nm) or equivalent energy of

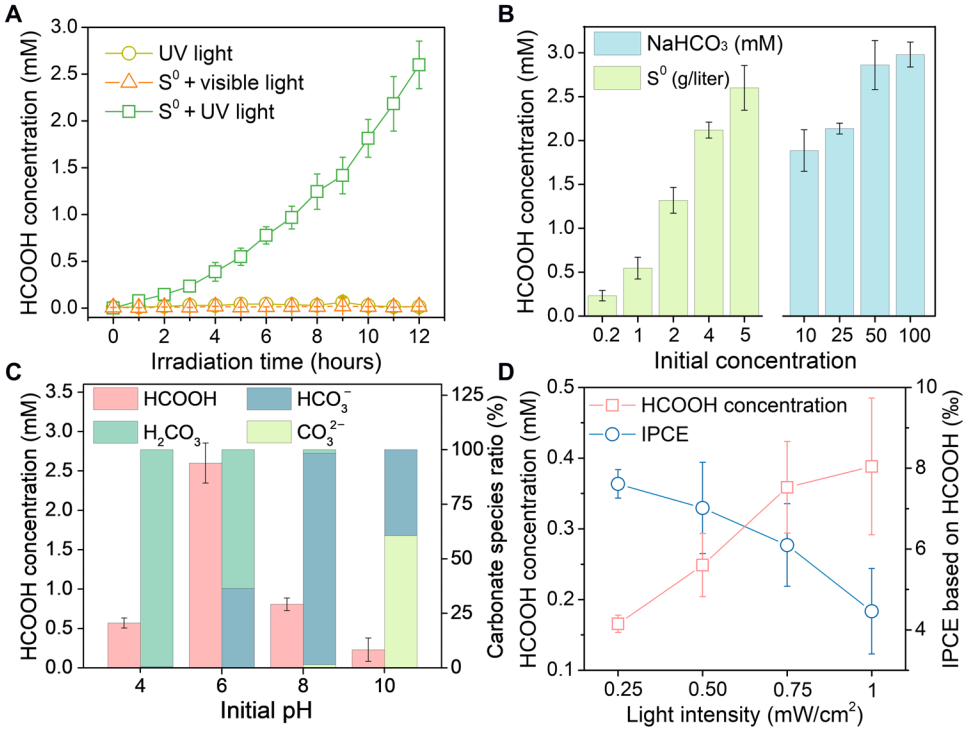

Fig. 2. The concentration of HCOOH varied with the following conditions. (**A**) Irradiation time in three control systems. (**B**) Different initial concentration of $NaHCO_3$ and S^0. (**C**) Different initial pH. (**D**) Different light intensity (254-nm UV light). Carbonate species ratios at corresponding pH values are illustrated in (C). IPCE under 254-nm irradiation based on HCOOH production is plotted in (D). Unless otherwise specified, the uniform reaction system contained S^0 (5 g/liter) and 50 mM $NaHCO_3$ at pH 6 and was irradiated for 12 hours in a wide UV-band mercury lamp.

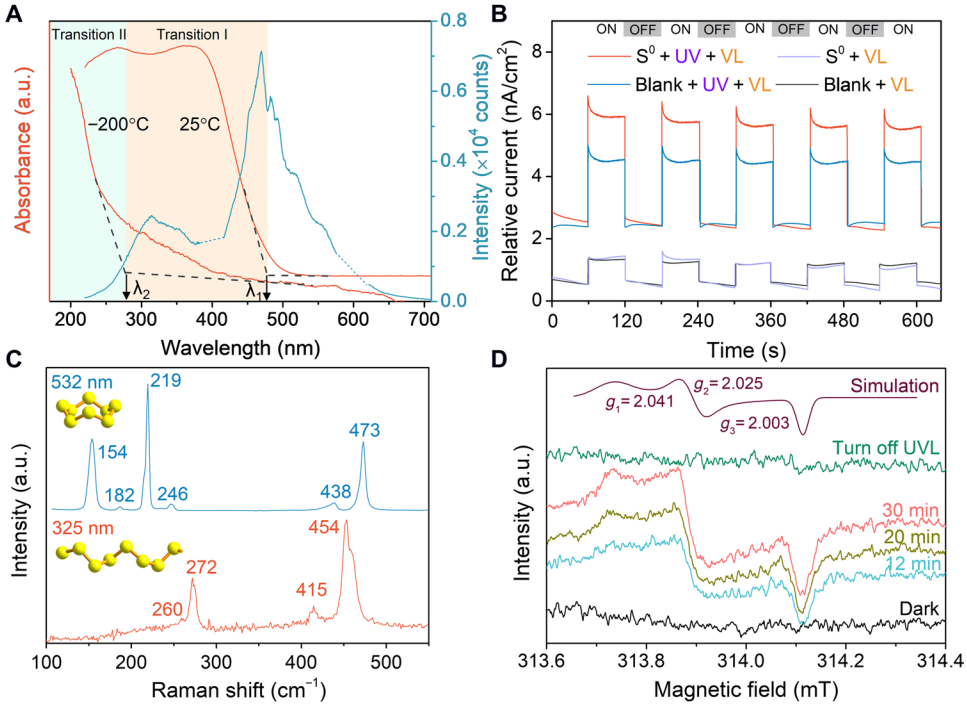

Fig. 3. Optical characteristics and bonding change of S^0 under UV light. (**A**) Absorption spectra (in black) at 25°C and −200°C, and room temperature emission spectrum (in blue) ranging from UV to visible band. The dashed lines in the emission spectrum curve were subtracted from the multiple-frequency peaks. (**B**) Recording of current changes under alternating on and off states of a xenon lamp [with UV and visible light (VL)] and the lamp with a UV filter, using S^0 or a blank substrate as electrodes. (**C**) Raman spectra recorded under 325- and 532-nm light irradiation, respectively. (**D**) Time-course EPR and the simulated spectra of S^0 under UV light.

photons higher than 2.6 eV. Transition II only responds to UV light (λ < 280 nm) with higher energy (4.4 eV) and is the direct mode. The indirect transition is phonon dependent and thus needs high enough temperature to generate phonons, leading to its inefficiency at low temperature (Fig. 3A).

Notably, the photo-generated electrons and holes are produced in the conduction band (CB) and valence band (VB), respectively. To confirm the formation of photo-generated carriers (electrons and holes) under light, photoelectrochemical measurements were performed on S^0 to compare the photocurrent change with and without light irradiation (Fig. 3B). Under xenon lamp (mainly visible light with 4% UV component), the current produced by S^0 (net current between the on and off state of the light) was 1.5-fold higher than the background current produced by the blank substrate. When the UV light was filtered, however, the photocurrents showed no notable difference between S^0 and the substrate, indicating that S^0 could not be excited without UV irradiation. Therefore, the effective electron transition only occurred in UV-excited direct mode rather than in the indirect mode, which can be attributed to the phonon-independent process of the former mode. According to the UV photoelectron spectra (fig. S3 and table S2), the VB and CB edges of S^0 were determined to be −6.86 and −2.46 eV [absolute vacuum energy scale (AVS)], respectively. This result is highly consistent with the recent DFT calculation (*34*). Accordingly, the redox potentials of CB electrons and VB holes were converted into −2.34 and 2.06 V [versus normal hydrogen electrode (NHE)] at pH 7, respectively.

Breaking of S—S bonds

The Raman spectrum of S^0 with the feature of homocyclic S_8 at 532 nm had stretching vibration modes at 438 and 473 cm^{-1} and bending modes at 154, 182, 219, and 246 cm^{-1} (Fig. 3C). When excited at 325 nm, however, a completely different spectrum that was assigned to the chain-like polymeric sulfur (denoted as S_μ) was recorded. Compared with the Raman bands of S_8, the frequencies of two stretching vibrations of S_μ decreased by 20 cm^{-1}, while those related to bending modes increased to 260 and 272 cm^{-1}. This was attributed to the longer bond length (2 pm) and decreased bond angle (2°) of S_μ than S_8 (*35*).

To further investigate the change of chemical bonds in S^0 under UV light, an in situ UV-irradiated electron paramagnetic resonance (EPR) measurement at −170°C was conducted. Some recorded signals (Fig. 3D), which gradually increased with UV exposure time, consisted of three components with anisotropic features. According to the *g* tensor values (g_1 = 2.041, g_2 = 2.025, and g_3 = 2.003), the simulated spectrum given in Fig. 3D was identical to the experimental one, indicating that the three signals were derived from a single paramagnetic radical. Notably, the radical was previously detected in a similar EPR measurement and reported to be the end of sulfur chain with a *trans* conformation (*36*). This confirmed that the chemical bonds between two sulfur atoms were broken under UV light and thus the homocyclic rings in S^0 were converted into chain-like S^0 allotropes (S_μ is one of the possible configurations). Notably, the EPR signals faded immediately when the light was turned off (Fig. 3D), which implied that the two short-lived dangling bonds would probably rebind and return to the initial state. Therefore, the fracture of the S—S bond, just like the excitation of photoelectrons, could only be activated by UV light.

Adsorption of carbonate molecules and formation of formate on S^0

In situ attenuated total reflection Fourier transform infrared spectroscopy (ATR-FTIR) was used to monitor the molecules on the surface of S^0 in UV-irradiated carbonate solution. It showed that

some peaks emerged after a long period of UV irradiation (Fig. 4). These features are mainly assigned to the monodentate carbonates or bicarbonates at 1518 cm^{-1} (collectively denoted as $HCO_3^-{}_{(ad)}$ due to HCO_3^- as the dominant species under this near-neutral condition), HCO_3^- (1419 and 1219 cm^{-1}), and HCOOH (1395 cm^{-1}) (*37*, *38*). The indication of carbonate molecules bonded on S^0 (i.e., $HCO_3^-{}_{(ad)}$), and the corresponding formation of HCOOH strongly confirmed the chemical adsorption of carbonate molecules on S^0 during their UV-induced photoreduction. There was no evidence for bonding of carbonate molecules on the surface of S^0 in the absence of UV light.

DISCUSSION

Reaction mechanisms based on the semiconducting properties of S^0

On the basis of the temperature-dependent optical absorption spectra (Fig. 3A) and DFT calculation (fig. S2), S^0 was characterized as an indirect semiconductor with two electronic transition modes, i.e., a phonon-independent direct one with a bandgap of 4.4 eV and a phonon-assisted indirect one with a bandgap of 2.6 eV. This is consistent with some previous spectroscopic studies (*39*, *40*). The photocurrent from UV-irradiated S^0 was high, while that produced under visible light was negligible (Fig. 3B), suggesting that the formation and transition of photoelectron-hole pairs in the UVC-induced direct transition were much more efficient than the indirect one excited by visible light, as described by Eq. 1.

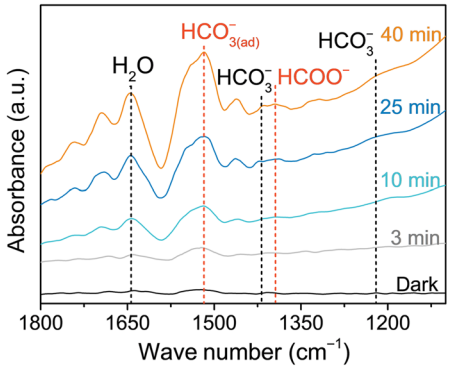

Fig. 4. ATR-FTIR spectra of molecules detected on the surface of S^0 in UV irradiation. The spectrum collected in the dark with no absorption feature remained unchanged for more than 30 min.

The band structure of S^0 is illustrated in Fig. 5A, in which the potentials of its VB, CB, and some redox couples are included for comparisons (see detailed values in tables S2 and S3). The reduction of CO_2 to HCOOH is widely accepted to be a multielectron transfer process (*41*). The formation of an active carbon(+IV) intermediate (denoted as $CO_2^{\cdot-}{}_{(ad)}$) after one single-electron transfer to the adsorbed CO_2 (denoted as $CO_{2(ad)}$; Eq. 2) is recognized as the rate-limiting step with a very negative potential of −1.9 V (versus NHE). $CO_2^{\cdot-}{}_{(ad)}$ could further accept one electron and two protons to finally yield HCOOH (Eq. 3). Notably, the energy potential of photoelectrons from S^0 is situated at −2.34 V (versus NHE at pH 7), much more negative than the potential for CO_2 activation (Eq. 2). The reduction of CO_2 is thus thermodynamically feasible by the photocatalysis of S^0. The results in Fig. 2C show that the maximum yield of HCOOH occurs in a slightly acidic environment (pH 6), confirming to some extent the significance of protons. Particularly, the concentration of S^0 oxidation products including sulfate (SO_4^{2-}) and sulfite (SO_3^{2-}) also increased with time in UV light (fig. S4), just as HCOOH behaved. Because the VB of S^0 is situated at 2.06 V (versus NHE at pH 7), much more positive than SO_3^{2-}/S^0 (−0.03 V) and SO_4^{2-}/SO_3^{2-} couples (−1.36 V) (*42*) (Fig. 5A), the photo-generated holes would undergo a successive two-step oxidation reaction that first oxidizes S^0 itself to SO_3^{2-} (Eq. 4 and Fig. 5B) and further to SO_4^{2-} (Eq. 5 and Fig. 5B). Because of the different rates of these two steps, S^0 and SO_3^{2-} constitute the competing hole scavengers, thus resulting in the lower concentration of SO_3^{2-} than SO_4^{2-} as shown in fig. S4. Reducing species like S^0 and SO_3^{2-}, if present in sufficient amounts in surrounding environments, thus not only serve as electron donors for CO_2 reduction but also help separate photoelectron-hole pairs to release free photoelectrons.

$$S^0 \xrightarrow{\lambda<280\ nm} e^- + h^+ \text{ (photoelectron-hole pair production)} \quad (1)$$

$$CO_{2(ad)} + e^- \rightarrow CO_2^{\cdot-}{}_{(ad)} \text{ (single-electron transfer to } CO_{2(ad)}) \quad (2)$$

$$CO_2^{\cdot-}{}_{(ad)} + e^- + 2H^+ \rightarrow HCOOH \text{ (proton-assisted electron transfer to } CO_2^{\cdot-}{}_{(ad)}) \quad (3)$$

$$S^0 + 4h^+ + 3H_2O \rightarrow SO_3^{2-} + 6H^+ \text{ (holes scavenged by } S^0) \quad (4)$$

$$SO_3^{2-} + 2h^+ + H_2O \rightarrow SO_4^{2-} + 2H^+ \text{ (holes scavenged by } SO_3^{2-}) \quad (5)$$

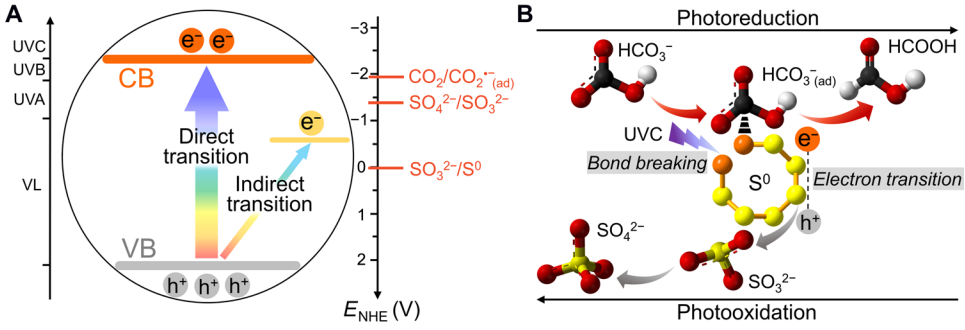

Fig. 5. Schematic of photocatalytic mechanism. (**A**) Band structure model of S^0 showing the two transition modes, and the redox potentials of VB, CB, and some related redox couples (versus NHE, pH 7). e^- and h^+ refer to photo-generated electrons and holes, respectively. Specific potential values are listed in tables S2 and S3. (**B**) Adsorption, activation, and photoreduction of carbonates by S^0 under UV light. For simplification, S^0 crystal is illustrated as a homocyclic S_8 molecule.

When the incident photon energy is not high enough for a direct transition but sufficient to cause an indirect transition (i.e., 280 nm < λ < 475 nm), only a few photoelectrons would be produced in the indirect band. This happens because the electron transition mode is phonon-assisted and thus has a small absorption coefficient (fig. S2). In this situation, the reduction of CO_2 is thermodynamically inhibited, and thus, no organic products can be produced.

Reaction mechanisms based on broken bonds reacting with adsorbed molecules

The S—S covalent bonds in S^0 can be broken by UV light (Fig. 3, C and D), as described in Eq. 6. Simultaneously, carbonate species can be adsorbed onto the surface of UV-irradiated S^0 (Fig. 4). All these observations suggest that the surface of S^0 would become quite active and highly absorbent to polar molecules and charged ions (e.g., HCO_3^- and CO_3^{2-}) once the nonpolar bonds are broken under UV light and become polar radicals, as shown in Fig. 5B and described by Eq. 7. The monodentate CO_3^{2-} or HCO_3^- is thus the actual adsorbed carbon(+IV) species on the surface of S^0. The recent DFT calculations reveal that the valence electrons of S_n species ($n \leq 8$) after chain cleavage from S_8 ring are dominantly localized at the terminal chain atoms (*34*). Such robust radicals on the surface of S^0 would potentially play dual roles in the aqueous carbonate system. On the one hand, the unpaired electrons of the radicals can be directly trapped by the adsorbed groups and thus assist the reduction of targeted molecules. On the other hand, these radicals preferentially adsorb charged HCO_3^- and CO_3^{2-}, and thus accelerate the indirect transfer of photoelectrons from S^0 to carbon(+IV) (Fig. 5B). From this point of view, an alkaline (pH > 8) environment gives rise to HCO_3^- and CO_3^{2-}, and thus might have been more beneficial to carbon(+IV) reduction than the acidic environment. However, the thermodynamic advantage from protons for carbon(+IV) reduction should be taken into consideration (Fig. 5A). In this case, a balance is achieved in that the weakly acidic carbonates containing H_2CO_3 and HCO_3^-, e.g., 64% H_2CO_3 and 36% HCO_3^- at pH 6, could produce the maximal amount of HCOOH (Fig. 2C).

$$-S-S- \xrightarrow{\text{UV light}} -S^{\cdot} + -S^{\cdot} \text{ (cleavage of sulfur bonds)} \quad (6)$$

$$-S^{\cdot} + HCO_3^- \rightarrow HCO_{3\,(ad)}^- \text{ (adsorption of charged carbonates)} \quad (7)$$

Implications for photoreactive S^0 in prebiotic terrestrial hydrothermal systems

Modern hydrothermal systems have been considered as a potential window to glance at the prebiotic Earth (*13*, *43*, *44*). We observed that solid S^0 mineral occurred abundantly in modern terrestrial hydrothermal systems, such as Tengchong in China (Fig. 1), Yellowstone National Park in United States (*23*), and other sites in Japan (*24*), Indonesia (*25*), and New Zealand (*26*). As the main comproportionation reaction product of H_2S, SO_2, and soluble sulfur species (*23*, *45*, *46*), S^0 minerals were abundant and widespread in the terrestrial hot springs and lakes in modern Earth. While drawing an analogy with modern cases and performing model simulations (*28*–*31*), the concentration of S^0 in early terrestrial hot springs was likely to be over μM level, by estimating from its sufficient sources including high-level atmospheric S^0 aerosol and dissolving sulfuric anions at μM to mM level. Different from primitive metal sulfides that precipitate mainly at deep-sea subduction zones and ridges (*22*), S^0 should be distributed primarily in the shallow photic zone of primitive hot springs due to its hydrophobicity and low density (*23*, *24*). Notably, in the primitive Earth, extreme UVC with an eightfold greater total flux than nowadays could penetrate an ozone-free atmosphere to reach the surface of Earth (*47*, *48*) and even reach the depth of several centimeters to meters in early ocean (*30*, *49*). Elemental sulfur in terrestrial hydrothermal systems and its absorption of extreme UVC could have laid the foundation for the occurrence of photocatalysis in the primitive Earth.

HCOOH is the main detectable organic species in the UV-irradiated system (Eqs. 2 and 3), where S^0 provided the reducing photoelectrons and was consumed by oxidation to sulfite and sulfate by a self-sacrifice catalytic process. As one of the most essential precursors in the abiotic synthesis of hydrocarbons (*50*, *51*), HCOOH could be produced from carbon(+IV) reduction by H_2 in analog submarine hydrothermal conditions (*19*, *51*). Our work shows that solar light can provide the energy required for the abiogenic reduction of carbon(+IV) in terrestrial hydrothermal systems where the temperature is less than 100°C. In particular, semiconducting minerals like S^0 are remarkable mediators by absorbing and converting solar energy into the chemical form. We can identify two advantages for this kind of energy-transforming pathway. On the one hand, the potential of photoelectrons from S^0 (−2.34 V versus NHE at pH 7) when excited by UVC is much more negative than that of H_2 (−0.42 V for H_2O/ H_2 couple at pH 7) and the photoelectrons from sulfide minerals like ZnS (−1.64 V) and MnS (−1.61 V) (*52*), providing S^0 with extraordinary reducing power for HCOOH synthesis. On the other hand, there were substantial reducing ionic species like S^0, SO_3^{2-}, S^{2-}, Fe^{2+}, and NO_2^- in the primitive ocean, which could not directly reduce carbon(+IV) under ordinary conditions due to thermodynamic energy barriers. After donating electrons to scavenge the photo-generated holes of UVC-excited S^0 (2.06 V versus NHE at pH 7), however, those electrons would be converted to highly reducing photoelectrons and thus surmount the energy barriers required for carbon(+IV) reduction. Based on this, it can be concluded that the weakly reducing species also contribute to carbon(+IV) reduction in systems that are exposed to sunlight and contain the mineral photocatalyst S^0.

To estimate the abiotic production of organic molecules and evaluate the role of S^0 proposed in this work, a simple model with S^0 particles suspended in the photic zone of the early terrestrial hot springs is assumed. The concentration of HCOOH produced each day (denoted as C_{HCOOH}, mM/day) is plotted against S^0 concentration (denoted as m_s, mM) in fig. S5, obtained in the experiment using simulated prebiotic conditions: 130 mM carbonate ions (*15*), pH 6.0 (*15*, *53*), and 6 $W \cdot m^{-2}$ UV flux ranging from 200 to 300 nm (*20*, *48*). After linear regression, the mathematical relationship between C_{HCOOH} and m_s is well described by linear Eq. 8. Furthermore, the estimation of the total yields (absolute quantity) of HCOOH is made by considering the thickness of the UVC photic zone (denoted as D_{UV}) and the area ratio of hot springs to the total surface of early Earth (denoted as A). The product of these two parameters determined the total volume of UVC-irradiated S^0 suspensions (more detailed information in Materials and Methods). Accordingly, the maximum mass of cumulative HCOOH depending on m_s, A, and D_{UV} is illustrated in Fig. 6, which is made based on Eq. 9. Notably, in a reasonable set of conditions represented by m_s (up to 10 μM), A (less than 10%), and D_{UV} (up to 1 m), the maximum

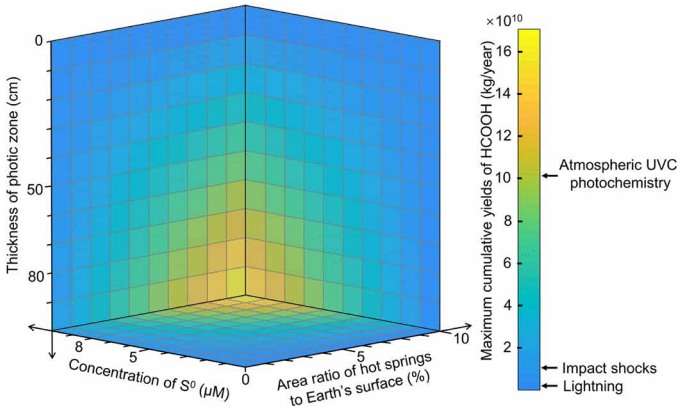

Fig. 6. Cumulative yields of HCOOH in the proposed model as a function of thickness of photic zone, concentration of S^0, and the area ratio of primitive terrestrial hot springs to Earth's surface. Some proposed main sources of abiogenic synthesis of organics are presented for comparison.

amount of HCOOH produced in this model is comparable to other organics with similar molecular weight like formaldehyde, hydrogen cyanide, and amino acids, which have been proposed from other abiogenic sources, e.g., atmospheric photochemistry, impact shocks, and lightning, respectively (*54*). For instance, if assuming the primitive terrestrial hot springs account for 1% of Earth's surface, S^0 at 10 μM would produce maximal 1.71×10^9 kg of HCOOH per year within 10-cm-thick photic zone. Note that the conversion of HCOOH to other complicated biomolecules has a moderate reducing potential like −0.11 V (versus NHE at pH 7) for methane and 0.07 V for acetic acid (*21*, *41*). The further synthesis of macromolecules based on HCOOH is thermodynamically favored under the photocatalysis of S^0. Furthermore, S^0 might also be involved in the so-called cyanosulfidic chemistry and contribute the yield of building blocks for life (*55*). Therefore, the extraordinarily reducing photoelectrons of S^0 could provide an alternative and efficient abiogenic pathway to produce biomolecules in primitive hot springs.

$$C_{HCOOH}(\text{mM/day}) = 0.02\, m_S \quad (8)$$

$$C_{HCOOH}(\text{kg/year}) = 1.71 \times 10^{12} D_{UV} \cdot m_S \cdot A \quad (9)$$

Terrestrial hydrothermal systems are distinguished by the everyday input of sufficient solar energy, multiple reducing ions as electron donors, and the abundant semiconducting minerals like S^0. By virtue of these conditions, the lower-temperature terrestrial hydrothermal systems could also support primordial carbon fixation and energy conversion, which are comparable to the traditional H_2-dependent pathways near high-temperature submarine hydrothermal vents. Moreover, the moderate temperatures in terrestrial hydrothermal systems and the absorption of extreme UV light by S^0 could prevent biomolecules from decomposition, providing suitable habitats for the incubation of primitive life. Besides the well-known clays, metals, and metal sulfides, S^0 thus turns out to be a newfound nonmetallic mineral catalyst that can enable the prebiotic synthesis and preservation of biomolecules. Beyond Earth, UV-activated S^0 minerals may also catalyze the conversion of inorganic carbon into organic molecules on exoplanets. On Mars, for example, siliceous sinter deposits were discovered by the rover Spirit (*56*, *57*), implying a terrestrial hydrothermal system in Martian surface and near-surface environments. The newly discovered photocatalysis of S^0 would provide a novel clue for seeking or detecting biomolecules and biosignatures.

MATERIALS AND METHODS

Preparation of S^0 samples

Natural samples collected from the hot springs were dried at 40°C for 12 hours and then ground into powders. Natural S^0 druses collected from the fumarole were selected in a stereoscope equipped with a 20× objective for roughly removing foreign materials. Commercial S^0 powders (99.9 weight %) were purchased from Sinopharm Chemical Reagent Beijing Company Limited. Single-crystal S^0 was from Geological Museum of Peking University, which was a natural sample but lacked exact information about its origin. Three types of S^0 film on different substrates were prepared. The S^0 film electrode on conductive glass (F-doped SnO_2, abbreviated as FTO) was prepared by spin-coating method: Commercial S^0 was first dissolved in carbon disulfide (CS_2). Then, a piece of 2.5 cm by 2.5 cm transparent FTO glass was spun using a spin coater (KW-4A, China) with a rate of 4000 rpm. S^0-saturated CS_2 solution was dripped onto the spinning FTO glass for 40 s, on which a thin S^0 film was left after the evaporation of CS_2. The second S^0 film was deposited on a single-crystal Ge that was already embedded into an ATR accessory. S^0-saturated CS_2 solution was dripped onto the Ge crystal, and the S^0 film was obtained after naturally evaporating CS_2. Another S^0 film on quartz glass was prepared by thermal evaporate plating method: Commercial S^0 powders were put into a tubular furnace and heated at 500°C. The produced hot sulfur vapor was flowed with the nitrogen to the unheated part, where a 2-mm-thick quartz wafer glass with 13 mm in diameter was put in advance. A thin S^0 film was obtained from the solidified sulfur vapor. The specific uses of each S^0 sample are shown in table S4.

Mineralogical identification and morphological observation of S^0 samples

Natural samples were identified using an x-ray diffractometer (X'Pert Pro MPD, PANalytical, The Netherlands) equipped with Cu Kα irradiation (λ = 1.5406 Å). The patterns were recorded from 5° to 85° (2θ) with a scanning speed of 2°/min.

Micro-Raman analysis was carried out on a spectrometer (inVia Reflex, Renishaw, UK) equipped with a 532-nm Nd:YAG laser and a 325-nm He-Cd laser. The beam was focused within 1 μm onto samples at the microscope stage through a ×50 objective.

The morphology of natural S^0 was observed by environmental SEM (Quanta 200FEG, FEI, USA) equipped with energy-dispersive X-ray spectroscopy detector at 15.0 kV. The colloidal solution in photochemical experiments was collected and dripped onto a holey carbon film supported by a Cu grid. After air-drying, the prepared sample was loaded into the holder of transmission electron microscope (Tecnai F20, FEI, USA) and observed at 200 kV. Digital micrograph version 3.6.5 (Gantan Ltd.) was applied for the image processing.

Optical and semiconducting characterization of S^0

The absorbance of S^0 powder sample at room temperature in 200 to 750 nm was detected on a spectrometer (UV-3600 Plus, Shimadzu, Japan) equipped with a diffuse integrating sphere attachment. $BaSO_4$ was used as a reference, and the slit width of the incident light was

2 nm. The absorbance of S^0 under low temperature was recorded in the transmission mode. S^0 was cooled to −200°C by liquid nitrogen, which was controlled by an intelligent temperature controller (MercuryiTC, Oxford Instruments, UK). The room temperature fluorescence was collected with an F-7000 FL spectrophotometer (Hitachi, Japan). The 200-nm exciting light passed through a 5-nm slit and reached the S^0 sample; the slit for the emitting light was 7 nm.

UV photoelectron spectroscopy of S^0 on FTO substrate was carried out on an ESCALAB 250Xi spectrometer (Thermo Fisher Scientific, USA) with HeI (21.22 eV) emission line used as the excitation source. The data were collected with a helium pressure of about 2×10^{-8} mbar in the analysis chamber and at −10 V bias.

The determination of energy levels of VB and CB for S^0

The work function (Φ) (Fermi level in vacuum) of S^0 was calculated by Eq. 10, where *hv* equals 21.22, and E_F and E_{cutoff} refer to the Fermi level and the kinetic energy of secondary electron cutoff, respectively. For calibration, the value of E_F was referenced to the measured value of an Au electrode, which directly contacted S^0 during the measurement. As shown in fig. S3, E_F (from referenced Au) and E_{cutoff} were estimated as 20.78 and 3.76 eV, respectively. The work function of S^0, based on Eq. 10, was estimated as 4.2 eV on the AVS. Therefore, its Fermi level was −4.20 eV (versus AVS), and the energy positions of VB edge (versus AVS) were calculated as −6.86 eV according to the gap between E_F and VB (2.66 eV). The CB edge (versus AVS) of S^0 was at −2.46 eV due to its direct bandgap of 4.4 eV.

Note that the energy levels of a semiconductor on the AVS correspond to those obtained in an electrolyte at the pH condition where its surface is zero charge (i.e., pH_{PZC}) (*52*, *58*). Therefore, the redox potentials of electrons in CB and holes in VB could be calculated based on Eqs. 11 and 12 (*52*), where E_{NHE} and E_{AVS} refer to potentials with respect to the NHE and energy levels on AVS, respectively, and E_{pH} is the potential at any given pH value. According to the pH_{PZC} value of S^0 (ca. 2.0) (*59*), potentials of electrons and holes for S^0 in aqueous electrolytes could be calculated as −2.34 and 2.06 V (versus NHE) at pH 7 (table S2).

$$hv - \Phi = E_F - E_{cutoff} \quad (10)$$

$$E_{NHE} = -E_{AVS} - 4.50 \quad (11)$$

$$E_{pH} = E_{PZC} + 0.059 \times (pH_{PZC} - pH) \quad (12)$$

Band structure calculation based on DFT

DFT-based first-principles calculation was performed using the Vienna Ab initio Simulation Package (VASP 5.4.4) (*60*) together with the ion-electron interaction described by the projector augmented wave method. Bandgap value was obtained with the HSE06 hybrid functional. A primitive cell of α-S with 32 atoms and six electrons ($3s^2 3p^4$) for valence electrons of each S atom were modeled. The Hartree-Fock mixing parameter and the cutoff energies of plane wave were set to the standard values of 25% and 340 eV, respectively. During VASP calculations, the gamma-centered *k*-point grid $4 \times 4 \times 4$ was used for geometry optimization. The force convergence criterion was set as 0.01 eV $Å^{-1}$ when the lattice parameters were relaxed, and the criterion for energy convergence when atomic positions were relaxed was set as 0.01 meV.

In situ experiments on S^0 on UV irradiation

In situ X-band EPR measurement was conducted on a JES-FA200 spectrometer (JEOL, Japan). A fraction of single-crystal S^0 was put into a quartz tube, and the sample chamber was cooled down to −170°C by liquid nitrogen. A high-pressure mercury lamp (USH-500SC, JEOL, Japan) was used to emit UV light. Each spectrum collection lasted 2 min, and time-course signals were recorded after the UV light was on.

In situ FTIR experiments were performed on a Vertex 70 spectrometer (Bruker, Germany) equipped with a horizontal Ge-based ATR accessory. Before the ATR-FTIR measurements, 1 ml of solution, which contained 50 mM $NaHCO_3$, was adjusted to pH 6 by H_3PO_4, and then dripped onto the prepared S^0 film on Ge crystal. A background spectrum was taken, and another spectrum was recorded using this background several minutes later to ensure that the system was in equilibrium. A high-pressure mercury lamp (CEL-M500, Aulight, China) was placed 10 cm over the ATR accessory. The UV light was on once the system was in equilibrium. During the irradiation, 64 scans at a resolution of 4 cm^{-1} in the range of 1000 to 4000 cm^{-1} were collected for each ATR-FTIR spectrum using OMNIC software.

Photocurrent measurements in an electrochemical system

Photocurrent measurements were carried out in a quartz glass reactor with three-electrode configuration using CHI 660C electrochemical apparatus (Chenhua, China). The prepared S^0 electrode, a platinum sheet (1 cm by 1 cm), and Ag/AgCl (3 M KCl) electrode were set as the working electrode, counter electrode, and reference electrode, respectively. The mixture of 0.5 M Na_2SO_4 and 0.5 M methanol was used as the electrolyte. The applied bias was set at 1.2 V (versus Ag/AgCl). An external xenon lamp (PLS-SXE300, Perfectlight, China) with simulated solar light spectrum directly irradiated the side of the working electrode without covering any S^0. The irradiation power density reaching the reactor was kept constant (6 mW/cm^2) after adding a UV filter. Lights on and off were controlled by the shielding separator in the same time period (60 s).

Photochemical experiments on carbonate reduction

Batches of experiments were carried out in simplified terrestrial hydrothermal conditions, in which only commercial S^0, sodium bicarbonate ($NaHCO_3$), pH, and UV light were considered. The reaction temperature was kept at ~35°C when irradiated with UV light. All preparation and sampling operations were performed in a glove box (Universal, MIKROUNA, China) filled with high-purity argon [the concentration of O_2 less than 0.1 parts per million (ppm)]. A quartz vessel reactor containing S^0, 50 ml of oxygen-free water, and $NaHCO_3$ was anaerobically sealed and fastened with an aluminum cap. Unless otherwise specified, the uniform conditions were set as S^0 (5 g/liter), 50 mM $NaHCO_3$ (pH 6), and irradiation for 12 hours in high-pressure mercury lamp (CEL-M500, Aulight, China). The pH was adjusted by 6 M H_3PO_4 and 1 M NaOH. The experimental and blank groups (without S^0 or light) were performed in triplicate. All reagents were of analytical grade and prepared using oxygen-free water. The oxygen-free water was prepared as follows: the distilled deionized water (18 megohm·cm) in a glass bottle was boiled for 20 min and then tightly sealed when it was boiling; it was then moved to the glove box for replacing the residual air with argon (99.999%) for 24 hours before use. In particular, several kinds of light sources were used for investigating the role of light wavelength in reactions, including wideband UV light from a mercury (Hg) lamp,

monochromatic UV light, wideband solar light from xenon lamp, and wideband visible light from a light-emitting diode lamp. The light intensity (table S5) and emission spectra (fig. S6) of all lamps were measured with a radiometer (FZ-A, Photoelectric Instrument Factory of Beijing Normal University, China) and a fiber spectrometer (S3000, Seemantech, China). The transmittance of quartz apparatus measured with a spectrometer (UV-3600 Plus, Shimadzu, Japan) is illustrated in fig. S7. More than 87% of UV light ranging from 250 to 380 nm, which was emitted from those lamps in experiments, would not be absorbed by the quartz apparatus.

Identification of products

The concentration of dissolved anions was determined by ion chromatography (ICS-1100, Thermo Fisher Scientific, MA, USA) with an IonPac AG14 Guard column and an AS14 analytical column with temperature of 30°C. The eluent was the mixture of 6 mM Na_2CO_3 and 5 mM $NaHCO_3$ with a flow rate of 1.0 ml/min. Standard curves of anions whose correlation coefficients all exceeded 0.999 were established before the measurement of samples.

^{1}H nuclear magnetic resonance (NMR) spectra were acquired using a 500-MHz Avance III spectrometer (Bruker, Germany) at room temperature. Generally, 0.25 ml of sample solutions was mixed with 0.05 ml of D_2O (99.9%; Sigma-Aldrich) and was placed in an NMR tube with 5-mm outside diameter. A solvent suppression was run to minimize the solvent signal, and 5 mM 3-(trimethylsilyl)-1-propanesulfonic acid-d6 sodium (DSS-d6; Sigma-Aldrich) was used for the calibration of the 0 ppm in advance.

Evaluation of photovoltaic efficiency

The IPCE in the photochemical experiment under monochromatic light was estimated according to the yield of HCOOH, using Eq. 13.

$$\mathrm{IPCE} = \frac{n_e}{n_p} = \frac{2 \times N_{\mathrm{HCOOH}} \times NA}{(P_{\mathrm{light}} \times t \times A)/(h\nu)} \quad (13)$$

where n_e, n_p, N_{HCOOH}, NA, P_{light}, t, A, h, and ν are the number of electrons for HCOOH production from CO_2, the number of incident photons, the mole number of produced HCOOH, Avogadro constant, the power of monochromatic light reaching reactor, irradiation time, the exposed area of reactor, Planck constant, and the frequency of monochromatic light, respectively.

Model description and the estimation of organic production

The model assumed that there were primitive carbonate terrestrial hot springs, whose area ratio (A, %) to the total surface area of early Earth (radius as 6371 km) was undetermined. Inside those springs, S^0 particles in a certain concentration (m_s, mM) were suspended in the UVC-penetrated photic zone with a certain thickness (D_{UV}, cm). On the basis of the above assumptions, the volume (V, m^3) of the photic zone in terrestrial hot springs is a function of A and D_{UV} (Eq. 14). Considering the relationship between daily HCOOH production (C_d, mM day^{-1}) and the concentration of S^0 (Eq. 8 and fig. S5), the annual production of HCOOH (C_y, kg $year^{-1}$) could be described as Eq. 15 (detailed form of Eq. 9) with respect to m_s, A, and D_{UV}.

$$V = 4\pi \times (6371 \times 10^3)^2 \times \frac{D_{\mathrm{UV}}}{100} \times A = 5.10 \times 10^{12} D_{\mathrm{UV}} A \quad (14)$$

$$C_y = V \times C_d \times 365 \times 46 \times 10^{-3} \quad (15)$$

SUPPLEMENTARY MATERIALS

Supplementary material for this article is available at http://advances.sciencemag.org/cgi/content/full/6/47/eabc3687/DC1

REFERENCES AND NOTES

1. H. C. Urey, On the early chemical history of the earth and the origin of life. *Proc. Natl. Acad. Sci. U.S.A.* **38**, 351–363 (1952).
2. L. E. Orgel, The origin of life on the earth. *Sci. Am.* **271**, 76–83 (1994).
3. V. M. Goldschmidt, Geochemical aspects of the origin of complex organic molecules on the Earth, as precursors to organic life. *New Biol.* **12**, 97–105 (1952).
4. W. Gilbert, Origin of life: The RNA world. *Nature* **319**, 618 (1986).
5. S. L. Miller, A production of amino acids under possible primitive earth conditions. *Science* **117**, 528–529 (1953).
6. G. Wächtershäuser, Groundworks for an evolutionary biochemistry: The iron-sulphur world. *Prog. Biophys. Mol. Biol.* **58**, 85–201 (1992).
7. A. Y. Mulkidjanian, A. Y. Bychkov, D. V. Dibrova, M. Y. Galperin, E. V. Koonin, Origin of first cells at terrestrial, anoxic geothermal fields. *Proc. Natl. Acad. Sci. U.S.A.* **109**, E821–E830 (2012).
8. S. Chatterjee, A symbiotic view of the origin of life at hydrothermal impact crater-lakes. *Phys. Chem. Chem. Phys.* **18**, 20033–20046 (2016).
9. B. Damer, D. Deamer, The hot spring hypothesis for an origin of life. *Astrobiology* **20**, 429–452 (2020).
10. D. J. Des Marais, M. R. Walter, Terrestrial hot spring systems: Introduction. *Astrobiology* **19**, 1419–1432 (2019).
11. K. O. Stetter, History of discovery of the first hyperthermophiles. *Extremophiles* **10**, 357–362 (2006).
12. C. L. Zhang, Q. Ye, Z. Huang, W. Li, J. Chen, Z. Song, W. Zhao, C. Bagwell, W. P. Inskeep, C. Ross, L. Gao, J. Wiegel, C. S. Romanek, E. L. Shock, B. P. Hedlund, Global occurrence of archaeal *amoA* genes in terrestrial hot springs. *Appl. Environ. Microbiol.* **74**, 6417–6426 (2008).
13. T. Djokic, M. J. Van Kranendonk, K. A. Campbell, M. R. Walter, C. R. Ward, Earliest signs of life on land preserved in ca. 3.5 Ga hot spring deposits. *Nat. Commun.* **8**, 15263 (2017).
14. M. Schoonen, A. Smirnov, Staging life in an early warm 'Seltzer' ocean. *Elements* **12**, 395–400 (2016).
15. J. W. Morse, F. T. Mackenzie, Hadean ocean carbonate geochemistry. *Aquat. Geochem.* **4**, 301–319 (1998).
16. R. M. Hazen, Life's rocky start. *Sci. Am.* **284**, 76–85 (2001).
17. M. Schoonen, A. Smirnov, C. Cohn, A perspective on the role of minerals in prebiotic synthesis. *Ambio* **33**, 539–551 (2004).
18. A. Lu, X. Wang, Y. Li, H. Ding, C. Wang, C. Zeng, R. Hao, X. Yang, Mineral photoelectrons and their implications for the origin and early evolution of life on Earth. *Sci. China Earth Sci.* **57**, 897–902 (2014).
19. M. Preiner, K. Igarashi, K. B. Muchowska, M. Yu, S. J. Varma, K. Kleinermanns, M. K. Nobu, Y. Kamagata, H. Tüysüz, J. Moran, W. F. Martin, A hydrogen-dependent geochemical analogue of primordial carbon and energy metabolism. *Nat. Ecol. Evol.* **4**, 534–542 (2020).
20. X. V. Zhang, S. T. Martin, C. M. Friend, M. A. A. Schoonen, H. D. Holland, Mineral-assisted pathways in prebiotic synthesis: Photoelectrochemical reduction of carbon (+ IV) by manganese sulfide. *J. Am. Chem. Soc.* **126**, 11247–11253 (2004).
21. X. V. Zhang, S. P. Ellery, C. M. Friend, H. D. Holland, F. M. Michel, M. A. A. Schoonen, S. T. Martin, Photodriven reduction and oxidation reactions on colloidal semiconductor particles: Implications for prebiotic synthesis. *J. Photochem. Photobiol. A* **185**, 301–311 (2007).
22. R. M. Hazen, D. Papineau, W. Bleeker, R. T. Downs, J. M. Ferry, T. J. McCoy, D. A. Sverjensky, H. Yang, Mineral evolution. *Am. Mineral.* **93**, 1693–1720 (2008).
23. Y. Xu, M. Schoonen, D. K. Nordstrom, K. Cunningham, J. W. Ball, Sulfur geochemistry of hydrothermal waters in Yellowstone National Park, Wyoming, USA. II. Formation and decomposition of thiosulfate and polythionate in Cinder Pool. *J. Volcanol. Geoth. Res.* **97**, 407–423 (2000).
24. B. Takano, H. Saitoh, E. Takano, Geochemical implications of subaqueous molten sulfur at Yugama crater lake, Kusatsu-Shirane volcano, Japan. *Geochem. J.* **28**, 199–216 (1994).
25. P. Delmelle, A. Bernard, M. Kusakabe, T. P. Fischer, B. Takano, Geochemistry of the magmatic–hydrothermal system of Kawah Ijen volcano, East Java, Indonesia. *J. Volcanol. Geoth. Res.* **97**, 31–53 (2000).
26. B. W. Christenson, S. White, K. Britten, B. J. Scott, Hydrological evolution and chemical structure of a hyper-acidic spring-lake system on Whakaari/White Island, NZ. *J. Volcanol. Geoth. Res.* **346**, 180–211 (2017).
27. H. L. DeWitt, C. A. Hasenkopf, M. G. Trainer, D. K. Farmer, J. L. Jimenez, C. P. McKay, O. B. Toon, M. A. Tolbert, The formation of sulfate and elemental sulfur aerosols under varying laboratory conditions: Implications for early earth. *Astrobiology* **10**, 773–781 (2010).

28. R. Hu, S. Seager, W. Bains, Photochemistry in terrestrial exoplanet atmospheres. II. H_2S and SO_2 photochemistry in anoxic atmospheres. *Astrophys. J.* **769**, 6 (2013).
29. M. Kumar, J. S. Francisco, Elemental sulfur aerosol-forming mechanism. *Proc. Natl. Acad. Sci. U.S.A.* **114**, 864–869 (2017).
30. J. F. Kasting, K. J. Zahnle, J. P. Pinto, A. T. Young, Sulfur, ultraviolet radiation, and the early evolution of life. *Origins Life Evol. B.* **19**, 95–108 (1989).
31. S. Ranjan, Z. R. Todd, J. D. Sutherland, D. D. Sasselov, Sulfidic anion concentrations on early earth for surficial origins-of-life chemistry. *Astrobiology* **18**, 1023–1040 (2018).
32. G. Liu, P. Niu, L. Yin, H.-M. Cheng, α-sulfur crystals as a visible-light-active photocatalyst. *J. Am. Chem. Soc.* **134**, 9070–9073 (2012).
33. R. Steudel, Das gelbe Element und seine erstaunliche Vielseitigkeit. *Chem. Unserer Zeit* **30**, 226–234 (1996).
34. J. Zhou, X. Liu, L. Zhu, S. Niu, J. Cai, X. Zheng, J. Ye, Y. Lin, L. Zheng, Z. Zhu, D. Sun, Z. Lu, Y. Zang, Y. Wu, J. Xiao, Q. Liu, Y. Zhu, G. Wang, Y. Qian, High-spin sulfur-mediated phosphorous activation enables safe and fast phosphorus anodes for sodium-ion batteries. *Chem* **6**, 221–233 (2020).
35. R. Steudel, B. Eckert, Solid sulfur allotropes. *Top. Curr. Chem.* **230**, 1–80 (2003).
36. R. Steudel, J. Albertsen, K. Zink, Photoinduced ESR signals in orthorhombic cyclo-octasulfur (α-S_8) and in quenched liquid sulfur at low temperatures. *Ber. Bunsen. Phys. Chem.* **93**, 502–509 (1989).
37. L. Liu, H. Zhao, J. M. Andino, Y. Li, Photocatalytic CO_2 reduction with H_2O on TiO_2 nanocrystals: Comparison of anatase, rutile, and brookite polymorphs and exploration of surface chemistry. *ACS Catal.* **2**, 1817–1828 (2012).
38. N. J. Firet, W. A. Smith, Probing the reaction mechanism of CO_2 electroreduction over Ag films via operando infrared spectroscopy. *ACS Catal.* **7**, 606–612 (2017).
39. B. E. Cook, W. E. Spear, The optical properties of orthorhombic sulphur crystals in the vacuum ultraviolet. *J. Phys. Chem. Solid* **30**, 1125–1134 (1969).
40. A. K. Abass, A. K. Hasen, R. H. Misho, Investigation of optically allowed transitions of α-sulfur thin films. *J. Appl. Phys.* **58**, 1640–1642 (1985).
41. S. N. Habisreutinger, L. Schmidt-Mende, J. K. Stolarczyk, Photocatalytic reduction of CO_2 on TiO_2 and other semiconductors. *Angew. Chem. Int. Ed.* **52**, 7372–7408 (2013).
42. J. A. Dean, *Lange's Handbook of Chemistry* (McGraw-Hill Inc., ed. 15, 1999).
43. W. Martin, J. Baross, D. Kelley, M. J. Russell, Hydrothermal vents and the origin of life. *Nat. Rev. Microbiol.* **6**, 805–814 (2008).
44. J. R. Michalski, T. C. Onstott, S. J. Mojzsis, J. Mustard, Q. H. S. Chan, P. B. Niles, S. S. Johnson, The Martian subsurface as a potential window into the origin of life. *Nat. Geosci.* **11**, 21–26 (2018).
45. Y. Xu, M. A. A. Schoonen, D. K. Nordstrom, K. M. Cunningham, J. W. Ball, Sulfur geochemistry of hydrothermal waters in Yellowstone National Park: I. The origin of thiosulfate in hot spring waters. *Geochim. Cosmochim. Acta* **62**, 3729–3743 (1998).
46. H. Kaasalainen, A. Stefánsson, Sulfur speciation in natural hydrothermal waters, Iceland. *Geochim. Cosmochim. Acta* **75**, 2777–2791 (2011).
47. V. M. Canuto, J. S. Levine, T. R. Augustsson, C. L. Imhoff, UV radiation from the young Sun and oxygen and ozone levels in the prebiological palaeoatmosphere. *Nature* **296**, 816–820 (1982).
48. C. S. Cockell, The ultraviolet history of the terrestrial planets—Implications for biological evolution. *Planet. Space Sci.* **48**, 203–214 (2000).
49. F. Garcia-Pichel, Solar ultraviolet and the evolutionary history of cyanobacteria. *Orig. Life Evol. Biosph.* **28**, 321–347 (1998).
50. M. A. Schoonen, Y. Xu, J. Bebie, Energetics and kinetics of the prebiotic synthesis of simple organic acids and amino acids with the FeS-H_2S/FeS_2 redox couple as reductant. *Orig. Life Evol. Biosph.* **29**, 5–32 (1999).
51. T. M. McCollom, J. S. Seewald, Experimental constraints on the hydrothermal reactivity of organic acids and acid anions: I. Formic acid and formate. *Geochim. Cosmochim. Acta* **67**, 3625–3644 (2003).
52. Y. Xu, M. A. A. Schoonen, The absolute energy positions of conduction and valence bands of selected semiconducting minerals. *Am. Mineral.* **85**, 543–556 (2000).
53. I. Halevy, A. Bachan, The geologic history of seawater pH. *Science* **355**, 1069–1071 (2017).
54. C. Chyba, C. Sagan, Endogenous production, exogenous delivery and impact-shock synthesis of organic molecules: An inventory for the origins of life. *Nature* **355**, 125–132 (1992).
55. D. D. Sasselov, J. P. Grotzinger, J. D. Sutherland, The origin of life as a planetary phenomenon. *Sci. Adv.* **6**, eaax3419 (2020).
56. S. W. Squyres, R. E. Arvidson, S. Ruff, R. Gellert, R. V. Morris, D. W. Ming, L. Crumpler, J. D. Farmer, D. J. Des Marais, A. Yen, S. M. McLennan, W. Calvin, J. F. Bell III, B. C. Clark, A. Wang, T. J. McCoy, M. E. Schmidt, P. A. de Souza Jr., Detection of silica-rich deposits on Mars. *Science* **320**, 1063–1067 (2008).
57. S. W. Ruff, J. D. Farmer, Silica deposits on Mars with features resembling hot spring biosignatures at El Tatio in Chile. *Nat. Commun.* **7**, 13554 (2016).
58. W.-J. Chun, A. Ishikawa, H. Fujisawa, T. Takata, J. N. Kondo, M. Hara, M. Kawai, Y. Matsumoto, K. Domen, Conduction and valence band positions of Ta_2O_5, TaON, and Ta_3N_5 by UPS and electrochemical methods. *J. Phys. Chem. B* **107**, 1798–1803 (2003).
59. S. Kelebek, T. Salman, G. W. Smith, An electrokinetic study of three coals. *Can. Metall. Quart.* **21**, 205–209 (1982).
60. G. Kresse, J. Furthmüller, Software VASP, Vienna (1999). *Phys. Rev. B* **54**, 169 (1996).

Acknowledgments: All the coauthors give their deep appreciation to Meixiang Zhu, who passed away during the revision of this work. Her contributions to this work were tremendous, in the absence of which our fieldwork would not have been possible. We thank X. Bai and Y. Chen for their dedications to the design and plotting of Figure 6. **Funding:** This work was supported by the National Natural Science Foundation of China (grant nos. 41872042, 91951114, 91851208, and 41522201). **Author contributions:** Yan Li and A.L. designed the study and conceived the idea for the paper. Yanzhang Li, Yan Li, Yi Liu, Y.W., A.L., J.W., H.J., and X.W. performed photochemical experiments. Yanzhang Li, B.W., and L.L. finished mineralogical and semiconducting characterization of samples. H.Y. performed bandgap DFT calculation. Yanzhang Li, Yan Li, A.L., and Yi Liu analyzed the data. M.Z., Yong Lai, Yan Li, Yanzhang Li, Y.W., and H.J. led the fieldwork and sample collection. Yanzhang Li and Yan Li wrote and revised the paper. J.D. helped polish the paper. Yan Li, H.D., Yong Lai, C.W., and A.L. discussed the focus of the work. All authors provided critical feedback on drafts of this paper and approved the final version. **Competing interests:** The authors declare that they have no competing interests. **Data and materials availability:** All data needed to evaluate the conclusions in the paper are present in the paper and/or the Supplementary Materials. Additional data related to this paper may be requested from the authors.

Submitted 21 April 2020
Accepted 5 October 2020
Published 18 November 2020
10.1126/sciadv.abc3687

Citation: Y. Li, Y. Li, Y. Liu, Y. Wu, J. Wu, B. Wang, H. Ye, H. Jia, X. Wang, L. Li, M. Zhu, H. Ding, Y. Lai, C. Wang, J. Dick, A. Lu, Photoreduction of inorganic carbon(+IV) by elemental sulfur: Implications for prebiotic synthesis in terrestrial hot springs. *Sci. Adv.* **6**, eabc3687 (2020).